Clin Neuroradiol (2013) 23:293–300
DOI 10.1007/s00062-013-0212-3

ORIGINAL ARTICLE

A Preliminary Study of Epilepsy in Children Using Diffusional Kurtosis Imaging

Yuzhen Zhang, Xu Yan, Yu Gao, Dongrong Xu, Jie Wu, Yuhua Li

Received: 1 November 2012 / Accepted: 3 February 2013 / Published online: 29 May 2013

Abstract
Objective To study brain abnormalities, in terms of non-Gaussian water diffusion properties using diffusional kurtosis imaging (DKI) in children with electroencephalography (EEG) confirmed epilepsy lateralized to both hemispheres.
Methods A total of 15 children with epileptiform waves on EEG in both hemispheres and 18 children as normal controls (NC) matched for age and sex were recruited. Data from DKI for all children were used to characterize non-Gaussian properties. Fractional anisotropy (FA), mean diffusivity (MD), and mean kurtosis (MK) maps were estimated from the DKI datasets. Voxel-based analyses (VBA) based on these measures were performed and compared between the epilepsy and NC groups.
Results The VBA showed abnormal regions in both white matter (WM) and gray matter (GM) in those with epilepsy. Analysis of FA values revealed that the abnormal regions were significant mainly in the left frontal and temporal lobes of the WM. Analysis of MD values revealed that differences were significant mainly in the right hemisphere of the limbic lobe, uncus, parahippocampal region, both in GM and WM of frontal and temporal lobes, and GM of the rectus of the left cerebrum. Finally, analysis of MK values revealed significant differences mainly in WM of the frontal lobes of both cerebrum, and GM and WM of the parietal lobe of the right cerebrum.
Conclusions These preliminary results suggest that DKI is sensitive for the characterization of diffusion abnormalities in both WM and GM of children with epilepsy.

Keywords Epilepsy · Children · Diffusional kurtosis imaging · Magnetic resonance imaging

The first two authors contributed equally to this work.

Y. Li (✉) · Y. Zhang · Y. Gao
Department of Radiology, Xin Hua Hospital Affiliated to Shanghai Jiaotong University School of Medicine, 1665 Kong Jiang Road, 200092 Shanghai, P. R. China
e-mail: liyuhua10@sina.com

Y. Zhang
e-mail: zhangyuzhen7@hotmail.com

Y. Gao
e-mail: gaoandyu@hotmail.com

X. Yan · D. Xu
Key Laboratory of Brain Functional Genomics, Key Laboratory of Magnetic Resonance, East China Normal University, 200062 Shanghai, China
e-mail: maxwell4444@hotmail.com

D. Xu
MRI Unit, Columbia University Department of Psychiatry, & New York State Psychiatric Institute, NYSPI Unit 74, 1051 Riverside Drive, New York 10032, USA
e-mail: xud@nyspi.columbia.edu

J. Wu
Department of Pediatrics, Xin Hua Hospital Affiliated to Shanghai Jiaotong University School of Medicine, 200092 Shanghai, P. R. China
e-mail: wujie_xhyy@hotmail.com

Introduction

Epilepsy is the second commonest neurological disease worldwide across all ages. The preferred diagnostic test is electroencephalography (EEG). Idiopathic epilepsy is the most frequent type in children, and constitutes those who do not demonstrate significant structural changes on conventional magnetic resonance image (MRI).

Diffusion-weighted MRI is a powerful tool for assessing tissue microstructure. Conventional MRI methods, such as diffusion tensor imaging (DTI) measure the diffusion properties of water molecules with the assumption that diffusion occurs in an unrestricted environment with a Gaussian probability distribution. In biological tissues, the cellular microarchitecture restricts water movement, causing the diffusion displacement probability distribution to deviate substantially from a Gaussian form. Diffusional kurtosis imaging (DKI) has been proposed as a new technique for characterizing non-Gaussian diffusion components, in addition to Gaussian components, and is increasingly used in human brain studies. Recent research has demonstrated that DKI is a more comprehensive model than DTI in terms of describing the complex properties of water diffusion in vivo [1–3]. The DKI model estimates diffusion and kurtosis coefficients, while DTI only provides diffusion coefficients. The kurtosis value has been shown to provide additional information compared to DTI, which reflects the complexity of brain microstructure [2, 4–7]. Thus, DKI can potentially improve the sensitivity and specificity of the characterization of neural tissue abnormalities. Moreover, the kurtosis coefficient provides information on microstructural integrity in both GM and WM, and can handle the situation of crossing fibers [2].

To our knowledge, only a few studies have reported the use of DKI in children with idiopathic epilepsy. Given the sensitivity of diffusion kurtosis to changes in tissue microstructure and possibly edema, replacement of axons with glial cells and astrocyte proliferation may all be associated with damage caused by seizure activity. We hypothesize that DKI may play an important role in detecting a significant difference in non-Gaussian water diffusion in GM and WM changes in epilepsy. To test this hypothesis, we investigated the value of diffusional kurtosis by studying diffusion abnormalities in children with epilepsy and comparing the results with those of normal controls (NC). We performed whole-brain voxel-based analyses, as all 15 cases of epilepsy had abnormal EEG signals.

Material and Methods

Participants

The study was approved by the Research Ethics Board in our hospital, and consent forms were signed by custodians of all children. The criteria of the case group for recruitment of children with epilepsy were: (1) clinically diagnosed epilepsy; (2) epileptiform activity localized to both sides of the hemispheres on EEG examination; (3) no other neurological disorders; and (4) no febrile seizures. A total of 18 age- and sex-matched children were recruited as normal controls. Additional inclusion criteria for the NC group were: (1) no record of a neurological disorder or brain injury; (2) normal hearing, vision and movement; and (3) normal conventional MRI findings.

The data included 15 patients (eight girls and seven boys) in the case group, and 18 healthy children in the NC group (ten girls and eight boys). The children were 3–11.9 years old in the case group with mean age of 6.88 ± 3.13 years, and 4.1–9.3 years old in the NC group with mean age of 6.41 ± 1.41 years. All subjects in both the groups were consecutively recruited between September 2009 and August 2011.

MRI Acquisition

Children who cannot fall asleep naturally were given 10% chloralhydrate 0.5 ml/kg, oral administration for sedation before MRI scan. Nine children in case group and eight children in the NC group were given 10% chloralhydrate 0.5 ml/kg orally, in the study.

The MRI acquisitions were performed on a 3.0-T MRI scanner (Signa, General Electric Medical Systems, Milwaukee, WI). Both DWI images with three *b*-values (0, 1,250, and 2,500 s/mm^2) and diffusion encoding vectors along 25 nonparallel directions for each nonzero *b*-value were acquired. The spin-echo echo-planar imaging sequence was used to acquire DWI images with the following parameters: TR/TE 14,000/76.9 ms, number of averages 1, slice thickness 2.5 mm, field of view (FOV) 24×16.8 cm^2, data matrix 96×96, imaging time 12 min and 8 s. Whole-brain T1-weighted magnetization-prepared rapid gradient echo (MPRAGE) images were acquired with: TI of 450 ms, TR/TE of 713/2.2 ms, flip angle 15°, one NEX, FOV of 24×24 cm^2, slice thickness 1 mm, 320×256 matrix, in approximately 3 min and 50 s. In addition, T2-weighted images were acquired for all children using a FLAIR sequence with the following parameters: TR/TE 8,002/153.9 ms, one NEX, slice thickness 5 mm, 18 slices, FOV 24×24 cm^2, 320×192 matrix, imaging time of approximately 1 min and 40 s. Sagittal fast spin-echo (FSE) images were acquired with: TR/TE of 2,560/116.6 ms, two NEX, FOV of 24×24 cm^2, slice thickness 3 mm, 384×224 matrix, in approximately 1 min and 15 s.

Data Analysis

Preprocessing

For all DWI images, we first corrected raw DWI data distortion induced by eddy current using the "eddy correct" tool in FSL, and removed nonbrain tissue using the BET tool (FSL). The apparent diffusion coefficient (ADC) and the apparent kurtosis coefficient (AKC) along each gradient

direction were estimated using the DWI data. Both MD and MK were subsequently calculated by averaging the ADC and the AKC along these directions. A diffusion tensor was then reconstructed at each voxel, and a fractional anisotropy (FA) map was estimated for each dataset. All estimations of DKI parameters were implemented using a software developed in-house.

Normalization

As suggested by Wilke et al. [8], attention needs to be paid to the spatial normalization of data from children, because of differences in size, composition, and shape between pediatric and adult brains. Thus, a pediatric template should be used instead of a conventional template in order to minimize the amount of deformation that can occur during spatial normalization and any possible errors. We created a subject-specific template using baseline DWI data (S0). The procedure consisted of three steps: (1) the creation of a template matched for age, of GM, WM, and cerebrospinal fluid (CSF) using the Template-O-Matic (TOM) toolbox [9] (http://dbm.neuro.uni-jena.de/software/tom/) The toolbox was developed from an NIH study of normal brain development [10], which arose from the structural data of 404 participants aged between 4.75 and 18.58 years, and it can generate high quality templates of T1-weighted data and tissue probability density for ages between 5 and 18; (2) normalization of the S0 images of all controls to the initial template using the unified segment method (SPM), which provides a probabilistic framework to combine image registration, tissue classification, and bias correction into a generative model [11]; and (3) averaging the normalized S0 images, smoothing the average with an 8 mm (full width at half maximum (FWHM)) Gaussian kernel, and thus obtaining our subject specific S0 template.

The S0 images of all participants were then nonlinearly registered to this template, using the normalizing tool in SPM, and the resulting deformation fields were applied to their corresponding FA, MD, and MK maps. Finally, all normalized parameter maps were smoothed with an 8 mm FWHM Gaussian kernel.

Statistical Analysis

We performed a voxel-based analysis for the entire brain on normalized and smoothed FA, MD, and MK maps. We applied a two-sample t test for group analysis between the 15 patients and the 18 healthy children in the NC. Contiguous voxels with a p-value <0.001 (uncorrected) and cluster size >100 were adopted to retain significant differences between the patient and NC groups.

Results

The data included 15 patients (eight girls and seven boys) in the case group, and 18 healthy children in the NC group. Characteristics of the 15 children with interictal epileptiform discharges (IED) located in bilateral hemispheres (No. 2–4, 6–8, 10, and No. 13, $n=8$), bilateral frontal lobes (No. 5 and No. 11, $n=2$), bilateral temporal lobes (No. 1 and No. 9, $n=2$), bilateral occipital lobes (No. 14, $n=1$), bilateral frontal-occipital areas (No. 12 and No. 15, $n=2$) can be seen in Table 1. There was no significant difference in average age between the case group (6.88 ± 3.13 years) and the NC group (6.41 ± 1.41 years), $p=0.5983$. The demographics and clinical characteristics of the epilepsy cases are shown in Table 1.

MRI findings in axial MPRAGE, T2W FLAIR and sagittal FSE sequences included a small lacunar focus in the left frontal lobe in patients No. 6, No. 11, No. 12, and in the frontal lobes bilaterally in patient No. 5. The other cases had normal conventional MRI findings.

Differences in FA regions between the two groups occurred mainly in the left cerebrum, WM and GM of the frontal and temporal lobes, the rectus, the frontal superior inferior orbital area, the caudate, the frontal gyrus, and the subcallosal gyrus. These differences can be seen in Table 2 and in Fig. 1a–c.

Differences in MD regions between the two groups occurred primarily in the cerebrum bilaterally, WM and GM of the limbic lobes, the uncus, the left frontal lobe, the rectus, the right temporal lobe, the parahippocampal area, and the rectus. These differences can be seen in Table 3 and in Fig. 2a–c.

Differences in MK regions between the two groups occurred mainly in both cerebral hemispheres, and several WM and GM regions of the frontal and parietal lobes. These differences can be seen in Table 4 and in Fig. 3a–c.

Discussion

Diffusion tensor imaging has been shown to provide unique structural information for the characterization of tissue microanatomy that cannot be achieved noninvasively or with other modalities. As a technique, DTI describes the process of tissue water diffusion using a second-order three-dimensional (3D) diffusivity tensor. Standard DTI indices include MD and FA. Diffusion properties of brain tissue demonstrated high sensitivity with WM integrity in both normal brains and those with pathological changes [12], and DTI has been used for the diagnosis of conditions such as cerebral ischemia [13], multiple sclerosis [14], schizophrenia [15], and brain tumors [16]. In epilepsy, reduced mean diffusivity has been shown in areas that EEG has indi-

Table 1 Demographic and clinical characteristics of 15 children with epilepsy

No.	Sex	Age (years)	Duration (years)	Ictal EEG findings	Seizure semiology
1	M	3	0.1	Spike, slow wave complex in temporal lobes bilaterally	Clonic limb movement, hypersalivation
2	F	4.8	1.8	Spikes, slow waves in hemispheres bilaterally, particularly the right temporal lobe	Clonic limb movement, hypersalivation
3	F	6	0.2	High amplitude spike, sharp, slow waves in hemispheres bilaterally	Clonic limb movement, hypersalivation
4	M	5	0.1	Occasional slow waves in hemispheres bilaterally	Clonic limb movement, eye open, fixed stare
5	F	6.5	0.7	Small amount of paroxysmal sharp, slow wave complex in bilateral frontal lobes	Clonic seizures of the right limbs
6	M	3.1	0.6	Paroxysmal sharp and slow waves in hemispheres bilaterally	Unconsciousness, fixed stare, hypersalivation
7	F	10.5	8	Sharp and slow wave complex in hemispheres bilaterally	Nocturnal seizure, clonic limb movement
8	M	6	0.1	Spikes, slow waves in hemispheres bilaterally, particularly the right median region	Clonic limb movement, eyes open, hypersalivation, unconsciousness
9	M	8.8	6	Paroxysmal sharp and spike waves in temporal lobes bilaterally	Clonic limb movement, hypersalivation, unconsciousness
10	M	4.2	0.1	Occasional paroxysmal spike and slow waves in hemispheres bilaterally	Clonic limb movement, hypersalivation
11	F	5.9	3	Paroxysmal spike and slow waves in frontal lobes bilaterally	Fixed stare
12	F	4.5	0.2	Paroxysmal spike and slow waves in fronto-occipital region bilaterally	Clonic limb movement, eyes open, fixed stare, unconsciousness
13	M	11.3	4	Sharp and slow waves in hemispheres bilaterally	Clonic limb movement
14	F	11.9	4	Occasional slow waves in occipital region bilaterally	Clonic limb movement, fixed stare
15	F	11.7	6	Paroxysmal spike and slow waves in bilateral frontal and Occipital region	Absence

MRI findings included a small lacunar focus in the left frontal lobe in patients No. 6, No. 11, No. 12, and in the frontal lobes bilaterally in patient No. 5. The other cases had normal conventional MRI findings

EEG electroencephalography, *F* female, *M* male

Table 2 Comparison of differences in FA in different regions between case and NC groups

No.	Region	MNI coordinate			Cluster size	*t* value
		x	y	z		
1	536 Left Cerebrum, 371 Frontal Lobe, 312 White Matter, 208 Gray Matter, 170 Rectus_L (aal), 167 Frontal_Sup_Orb_L (aal), 137 Caudate_L (aal), 123 Inferior Frontal Gyrus, 119 Subcallosal Gyrus, 105 Anterior Cingulate, 105 Limbic Lobe, 85 Medial Frontal Gyrus, 77 Brodman area 25, 72 Brodman area 47, 60 Sub-lobar	−10.1	20.64	−12	536	4.683452
2	370 Left Cerebrum, 370 Frontal Lobe, 346 White Matter, 255 Frontal_Inf_Orb_L (aal), 237 Middle Frontal Gyrus, 133 Inferior Frontal Gyrus, 67 Frontal_Inf_Tri_L (aal)	−35.48	36.62	−4.5	370	4.544104
3	232 Temporal Lobe, 232 White Matter, 232 Left Cerebrum, 197 Temporal_Mid_L (aal), 193 Middle Temporal Gyrus	−47.7	−52.68	0.5	232	4.808389

The results of cluster sizes > 50 for each region are shown in Tables 2, 3 and 4

The numbers before every region represent the cluster size for that region

The x, y, z of MNI coordinates, cluster size and *t* values in Tables 2, 3 and 4 reflect the largest difference between the case and NC groups points

MNI Montreal Neurological Institute

cated as being associated with seizure activity [17]. Studies have addressed the usefulness of DTI in epilepsy and have demonstrated increased diffusivity and reduced FA in areas corresponding to the electric focus [12, 18, 19]. Increased diffusivity and reduced FA have been demonstrated with DTI in the hippocampus of patients with temporal lobe epi-

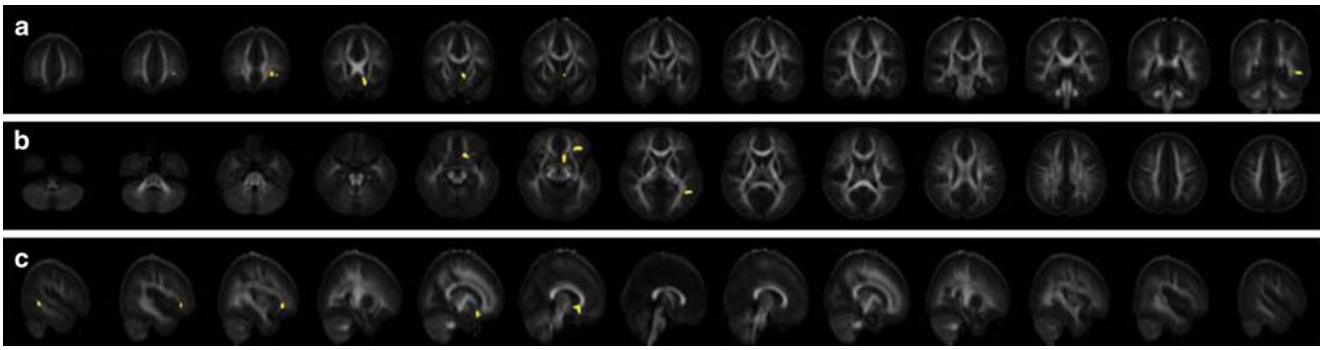

Fig. 1 Coronal (**a**), axial (**b**), and sagittal (**c**) images of FA maps. *Yellow* regions indicate significant differences between epilepsy and NC groups

Table 3 Comparison of differences in MD in different regions between case and NC groups

No.	Region	MNI coordinate			Cluster size	*t* value
		x	y	z		
1	374 Right Cerebrum, 365 Limbic Lobe, 247 Uncus, 239 ParaHippocampal_R (aal), 218 White Matter, 128 Gray Matter, 118 Parahippocampa Gyrus, 94 Fusiform_R (aal), 79 Brodman area 36	24.679999	−4.74	−37	387	−5.14674
2	118 Frontal Lobe, 118 Right Cerebrum, 92 Gray Matter, 80 Inferior Frontal Gyrus, 64 Frontal_Sup_Orb_R (aal), 62 Brodman area 11, 54 Rectus_R (aal)	13.399999	28.16	−22	118	−4.53022
3	277 Rectus_L (aal), 273 Frontal Lobe, 225 Left Cerebrum, 210 Medial Frontal Gyrus, 196 Gray Matter, 128 Brodman area 25, 68 Brodman area 11, 63 Rectal Gyrus, 57 White Matter	−3.520001	24.4	−22	322	−5.48334
4	267 Temporal Lobe, 267 Right Cerebrum, 251 Middle Temporal Gyrus, 206 White Matter, 117 Occipital_Mid_R (aal), 52 Temporal_Mid_R (aal)	46.299999	−70.54	25.5	267	−4.36779

MNI Montreal Neurological Institute

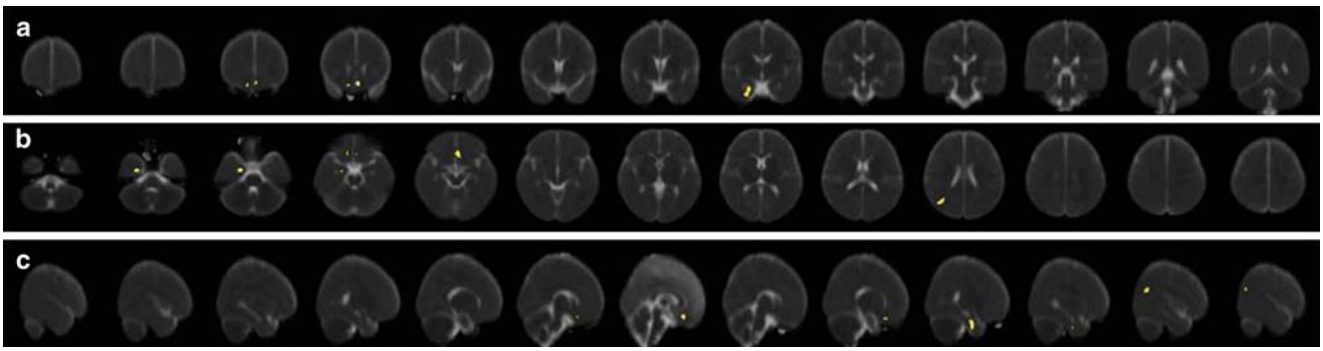

Fig. 2 Coronal (**a**), axial (**b**), and sagittal (**c**) images of MD maps. *Yellow* regions indicate significant differences between epilepsy and NC groups

lepsy (TLE) [17], in patients with malformations of cortical development, which is commonly associated with epilepsy [19], and in the hippocampus of patients with hippocampal sclerosis [20].

Despite this, conventional DTI does not fully utilize the MR diffusion measurements inherent to tissue microstructure. It implicitly assumes that water molecule diffusion occurs in a free and unrestricted environment with a Gaussian distribution of diffusion displacement. In biological tissues, water diffusion restriction in vivo is a complex process with numerous potential determinants, such as cell structures, restricted intra- or extra-cellular compartments, permeability or water exchange, and other biophysical properties associated with different water molecule populations that also potentially hinder and restrict diffusion. Although DTI is an important technique for investigating mechanisms of health and disease in brain WM, there are limitations, which including a lack of specificity in terms of histological features [21]. The simplified description of the diffusion process prevents DTI from being truly effective for the char-

Table 4 Comparison of differences in MK in different regions between case and NC groups

No.	Region	MNI coordinate			Cluster size	*t* value
		x	y	z		
1	82 Fusiform_L (aal), 50 Limbic Lobe, 50 Uncus, 50 Left Cerebrum	−25.14	−7.56	−39.5	108	5.310458
2	364 Left Cerebrum, 364 Frontal Lobe, 329 White Matter, 273 Middle Frontal Gyrus, 126 Frontal_Inf_Orb_L (aal), 71 Frontal_Inf_Tri_L (aal), 51 Frontal_Mid_Orb_L (aal)	−29.84	37.56	−4.5	364	4.309091
3	173 Frontal Lobe, 173 Right Cerebrum, 173 White Matter, 148 Middle Frontal Gyrus, 141 Frontal_Inf_Tri_R (aal)	45.359999	30.04	28	173	4.408129
4	104 Right Cerebrum, 88 Frontal Lobe, 87 Medial Frontal Gyrus, 68 White Matter	16.219999	39.44	28	104	4.140552
5	122 Pariet Lobe, 122 Right Cerebrum, 120 SupraMarginal_R (aal), 98 Inferior Parietal Lobule, 61 Gray Matter, 56 White Matter	49.119999	−34.82	38	122	4.094243

MNI Montreal Neurological Institute

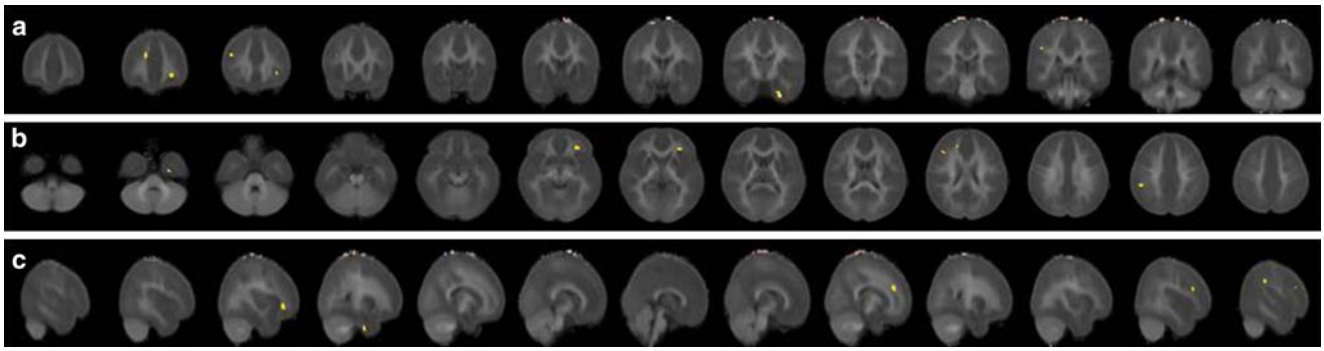

Fig. 3 Coronal (**a**), axial (**b**), and sagittal (**c**) images of MK maps. *Yellow* regions indicate significant differences between epilepsy and NC groups

acterization of relatively isotropic tissue in GM structures, such as the cortex, the hippocampus, and the basal ganglia, and the inability of DTI-based fiber tractography to resolve fiber crossings.

Diffusional kurtosis imaging has been proposed as a minimal extension of DTI, and has been recently developed to probe non-Gaussian diffusion properties [1, 2, 6]. It is a more comprehensive model for describing the restricted diffusion process in vivo, and could lead to improved neural characterization with better sensitivity and directional specificity. Thus, DKI is a potentially valuable tool for probing pathological alterations in neural tissues. In order to study density changes in GM, voxel-based morphometry (VBM) is commonly used. Thus far, DKI has demonstrated promising results in several brain conditions, including attention deficit and hyperactivity disorder [22], Parkinson's disease [23], Alzheimer's disease [24], schizophrenia [25], traumatic brain injury [26, 27], stroke [28], as well as in the staging of gliomas [29]. In these studies, DKI has proven to be a more sensitive tool for the detection and characterization of subtle changes in both WM and GM. It has also been explored in terms of resolving the crossing of WM fibers, thereby potentially leading to more accurate tracking and characterization [2, 30].

A typical DKI brain protocol acquires DWI images with a *b*-value of 6 (maximum *b*-value at 2,000–2,500 s/mm^2) and along more than 15 different directions. Diffusion of water protons in tissue is typically characterized by MD, which measures the average distance a water molecule traverses within a given observation time. A further parameter that is frequently derived from DTI data is FA, which provides information on the degree of diffusion anisotropy that exists within a given voxel. The axial diffusivity (AD or $MD_{\parallel}$) and radial diffusivity (RD of $MD_{\perp}$) provide further insights into the nature of the microstructural changes. The MK is a dimensionless index that quantifies the deviation of the water diffusion displacement profile from the Gaussian distribution, and measures the degree of diffusion hindrance or restriction [5, 6, 29]. The average apparent kurtosis along all diffusion gradient encoding directions has been measured and shown to offer an improved sensitivity for the detection of developmental and pathological changes in neural tissues compared to conventional DTI. Studies of brain maturation have shown that MK is sensitive to changes in GM, where MK increases with brain maturation; whereas, DTI parameters, MD and FA, remain relatively unchanged. The increase in MK observed during maturation in GM and WM is likely to be due to consistent and continuing myelination, an over-

all increase in microstructural complexity, and increased cell-packing density, particularly in GM [4].

In our study, EEG revealed spike, sharp, and slow wave complexes in the hemispheres bilaterally ($n=8$), and spike and slow wave complexes in the temporal lobes ($n=2$) and frontal lobes ($n=2$) bilaterally. Occasional slow waves were observed in the occipital region on both sides ($n=1$), and paroxysmal spike and slow waves in the fronto-occipital region bilaterally ($n=2$). The t test revealed more precise regions of anomalies in both, the case and NC groups in FA, MD and MK, in WM and GM, according to the EEG findings. Our results showed that in children with bilateral epilepsy, there was a significant reduction in FA in the left cerebrum of several WM and GM regions compared to NCs, for example, the frontal and temporal lobes, the rectus, the frontal superior/inferior orbital, the caudate, the frontal gyrus, and the subcallosal gyrus. In addition, it is clear from our data that this reduction was due to a significant increase in MD in several WM and GM regions of the cerebrum bilaterally, such as the limbic lobe, the uncus, the left frontal lobe, the rectus, the right temporal lobe, the parahippocampal region, and the rectus. There was a significant reduction in MK in both cerebral hemispheres and several WM and GM regions of the frontal and parietal lobes, indicating that MK is sensitive to changes in tissue microstructure secondary to epilepsy. These regions of reduced FA, increased MD, and reduced MK could reflect myelin deficiency, increased permeability in the axon membranes, or a less tightly packed neuronal network.

In experimental studies, repeated seizures cause neuronal damage and cell death [31]. However, in addition to neuronal death, changes such as axonal demyelination, formation of axonal spines, increase in interstitial fluid volume due to edema, replacement of axons with glial cells, and astrocyte proliferation can be associated with the damage induced by seizure activity. In all these situations, changes related to water diffusion are mostly in the direction of a loss of anisotropy. This loss of anisotropy could be due to decreased parallel diffusivity, increased perpendicular diffusivity, or a combination of the two. While the relationship between the pathophysiology of epilepsy and decreased anisotropy due to a variety of degenerative changes is well established, more precise mechanisms in terms of parallel/perpendicular diffusivity remain poorly understood. Mechanisms such as axonal swelling may preferentially increase the perpendicular diffusivity without decreasing parallel diffusivity. These diffusion changes could be the result of progressive degenerative changes occurring in the epileptic cortex and in the underlying WM as a result of persistent seizures.

Few studies have reported DKI in children with epilepsy. However, there are several limitations to the present study. The sample size was relatively small, and larger sample sizes with long-term prospective follow-up assessments are needed to confirm our findings. The two-sample t test statistical analysis method revealed overall rather than individual differences. The duration of epilepsy as well as seizure frequency or type may be associated with changes in diffusion, and a more detailed study is needed to assess these relationships. The matrix resolution of 96×96 in the present study is probably too rough to detect diffusion changes in small areas like the optic chiasm, lateral geniculate nucleus (LGN), and hippocampus. Increased matrix size will be selected in the follow-up study.

Given that cellular WM and/or GM microstructures are altered in many diseases, DKI is potentially applicable to a variety of neurological disorders, such as ischemic stroke, both WM and GM abnormalities in MS, Parkinson's disease, Alzheimer's disease, and other forms of degenerative dementia and brain tumors under both preclinical and clinical settings. It should be noted that the number of such DKI investigations remain limited, and more comprehensive studies are needed to further validate and explore the merits of the DKI approach for the characterization of various neural tissue alterations.

Conclusions

By quantifying FA, MD and MK, DKI may provide improved sensitivity and specificity for the characterization of microstructural complexities of neural tissues. The DKI method could greatly advance basic and clinical brain investigations by providing unprecedented micro-anatomical information from studies of WM and GM, particularly in those with epilepsy and normal brain imaging on conventional MRI.

Conflict of interest The authors declare that there is no actual or potential conflict of interest in relation to this article.

References

1. Jensen JH, Helpern JA, Ramani A, Lu H, Kaczynski K. Diffusional kurtosis imaging: the quantification of non-Gaussian water diffusion by means of magnetic resonance imaging. Magn Reson Med. 2005;53:1432–40.
2. Lu H, Jensen JH, Ramani A, Helpern JA. Three-dimensional characterization of non-gaussian water diffusion in humans using diffusion kurtosis imaging. NMR Biomed. 2006;19:236–47.
3. Jensen JH, Helpern JA. MRI quantification of non-Gaussian water diffusion by kurtosis analysis. NMR Biomed. 2010;23:698–710.
4. Cheung MM, Hui ES, Chan KC, Helpern JA, Qi L, Wu EX. Does diffusion kurtosis imaging lead to better neural tissue characterization? A rodent brain maturation study. Neuroimage. 2009;45:386–92.
5. Falangola MF, Jensen JH, Babb JS, Hu C, Castellanos FX, Di Martino A, et al. Age-related non-Gaussian diffusion patterns in the prefrontal brain. J Magn Reson Imaging. 2008;28:1345–50.

6. Hui ES, Cheung MM, Qi L, Wu EX. Towards better MR characterization of neural tissues using directional diffusion kurtosis analysis. Neuroimage. 2008;42:122–34.
7. Fieremans E, Jensen JH, Helpern JA. White matter characterization with diffusional kurtosis imaging. Neuroimage. 2011;58:177–88.
8. Wilke M, Schmithorst VJ, Holland SK. Assessment of spatial normalization of whole-brain magnetic resonance images in children. Hum Brain Mapp. 2002;17:48–60.
9. Wilke M, Holland SK, Altaye M, Gaser C. Template-O-Matic: a toolbox for creating customized pediatric templates. Neuroimage. 2008;41:903–13.
10. Evans AC, Brain Development Cooperative Group. The NIH MRI study of normal brain development. Neuroimage. 2006;30:184–202.
11. Ashburner J, Friston KJ. Unified segmentation. Neuroimage. 2005;26:839–51.
12. Arfanakis K, Hermann BP, Rogers BP, Carew JD, Seidenberg M, Meyerand ME. Diffusion tensor MRI in temporal lobe epilepsy. Magn Reson Imaging. 2002;20:511–9.
13. Lythgoe MF, Busza AL, Calamante F, Sotak CH, King MD, Bingham AC, et al. Effects of diffusion anisotropy on lesion delineation in a rat model of cerebral ischemia. Magn Reson Med. 1997;38:662–8.
14. Werring DJ, Clark CA, Barker GJ, Thompson AJ, Miller DH. Diffusion tensor imaging of lesions and normal-appearing white matter in multiple sclerosis. Neurology. 1999;52:1626–32.
15. Lim KO, Hedehus M, Moseley M, de Crespigny A, Sullivan EV, Pfefferbaum A. Compromised white matter tract integrity in schizophrenia inferred from diffusion tensor imaging. Arch Gen Psychiatry. 1999;56:367–74.
16. Price SJ, Peña A, Burnet NG, Jena R, Green HA, Carpenter TA, et al. Tissue signature characterisation of diffusion tensor abnormalities in cerebral gliomas. Eur Radiol. 2004;14:1909–17.
17. Assaf BA, Mohamed FB, Abou-Khaled KJ, Williams JM, Yazeji MS, Haselgrove J, et al. Diffusion tensor imaging of the hippocampal formation in temporal lobe epilepsy. AJNR Am J Neuroradiol. 2003;24:1857–62.
18. Rugg-Gunn FJ, Eriksson SH, Symms MR, Barker GJ, Duncan JS. Diffusion tensor imaging of cryptogenic and acquired partial epilepsies. Brain. 2001;124:627–36.
19. Eriksson SH, Rugg-Gunn FJ, Symms MR, Barker GJ, Duncan JS. Diffusion tensor imaging in patients with epilepsy and malformations of cortical development. Brain. 2001;124:617–26.
20. Liacu D, de Marco G, Ducreux D, Bouilleret V, Masnou P, Idy-Peretti I. Diffusion tensor changes in epileptogenic hippocampus of TLE patients. Neurophysiol Clin. 2010;40:151–7.
21. Wu EX, Cheung MM. MR diffusion kurtosis imaging for neural tissue characterization. NMR Biomed. 2010;23:836–48.
22. Helpern JA, Adisetiyo V, Falangola MF, Hu C, Di Martino A, Williams K, et al. Preliminary evidence of altered gray and white matter microstructural development in the frontal lobe of adolescents with attention-deficit hyperactivity disorder: a diffusional kurtosis imaging study. J Magn Reson Imaging. 2011;33:17–23.
23. Wang JJ, Lin WY, Lu CS, Weng YH, Ng SH, Wang CH, et al. Parkinson disease: diagnostic utility of diffusion kurtosis imaging. Radiology. 2011;261:210–7.
24. Lu H, Jensen JH, Hu C, Falangola MF, Ramani A, Ferris S, et al. Alterations in cerebral microstructual integrity in normal aging and in Alzheimer's disease: a multi-contrast diffusion MRI study. Proc Intl Soc Mag Reson Med. 2006;14:723.
25. Ramani A, Jensen JH, Szulc KU, Ali.O, Hu.C, Lu.H, et al. Assessment of abnormalities in the cerebral microstructure of schizophrenia patients: a diffusional kurtosis imaging study. Proc Intl Soc Mag Reson Med. 2007;15:648.
26. Grossman EJ, Ge Y, Jensen JH, Babb JS, Miles L, Reaume J, et al. Thalamus and cognitive impairment in mild traumatic brain injury: a diffusional kurtosis imaging study. J Neurotrauma. 2012;29:2318–27.
27. Zhuo J, Xu S, Proctor JL, Mullins RJ, Simon JZ, Fiskum G, et al. Diffusion kurtosis as an in vivo imaging marker for reactive astrogliosis in traumatic brain injury. Neuroimage. 2012;59:467–77.
28. Jensen JH, Falangola MF, Hu C, Tabesh A, Rapalino O, Lo C, Helpern JA. Preliminary observations of increased diffusional kurtosis in human brain following recent cerebral infarction. NMR Biomed. 2011;24:452–7.
29. Raab P, Hattingen E, Franz K, Zanella FE, Lanfermann H. Cerebral gliomas: diffusional kurtosis imaging analysis of microstructural differences. Radiology. 2010;254:876–81.
30. Hori M, Fukunaga I, Masutani Y, Taoka T, Kamagata K, Suzuki Y, et al. Visualizing non-gaussian diffusion: clinical application of q-space imaging and diffusional kurtosis imaging of the brain and spine. Magn Reson Med Sci. 2012;11:221–33.
31. Kotloski R, Lynch M, Lauersdorf S, Sutula T. Repeated brief seizures induce progressive hippocampal neuron loss and memory deficits. Prog Brain Res. 2002;135:95–110.